ACS Partner Journal

CHEM & BIO ENGINEERING

pubs.acs.org/ChemBioEng

Article

Deciphering Metal–Organic Framework Synthesis from Hydroxy Double Salts: In-Situ Insights via Synchrotron X-ray Diffraction and Absorption Spectroscopy

Ming Zhang, Xinyu Luo, Yubin Hu, Yuanhao Shen, Yixin Chen, Shuchang Yuan, Hao Wang, Xueqing Xing, and Junjie Zhao*

Cite This: *Chem Bio Eng.* 2024, 1, 606–614

Read Online

ACCESS | Metrics & More | Article Recommendations | Supporting Information

ABSTRACT: Developing rapid room-temperature synthesis is key to sustainable manufacturing of metal–organic frameworks (MOFs). Using layered compounds such as hydroxy double salts (HDSs) as precursors significantly promotes the reaction kinetics and lowers the required synthesis temperature. However, limited understanding of the reaction mechanism impedes the further exploration of new routes for MOF synthesis. Here, we report for the first time the use of combined in-situ synchrotron X-ray diffraction and X-ray absorption spectroscopy to monitor the dynamic processes to form MOFs in solution. The conversion from a (Zn,Co) HDS to a mixed-metal zeolitic imidazolate framework-8 (mmZIF-8) was chosen as our model reaction. Time-resolved diffraction patterns exclude the presence of intercalated HDS structures with altered *d*-spacing and any other crystalline intermediate phase during the synthesis. The activation energies of nucleation and growth were found as 25.5 ± 2.5 and 64.0 ± 7.9 kJ·mol^{-1}, respectively. In addition, we captured the evolution of local structures from mixed coordination states in the HDS to tetrahedral coordination in the mmZIF-8. Furthermore, two possible reaction pathways were proposed to account for the fast conversion from HDS to mmZIF-8. The fundamental understanding towards the HDS-based synthesis obtained in this work is expected to guide future development of new fabrication methods for MOF materials.

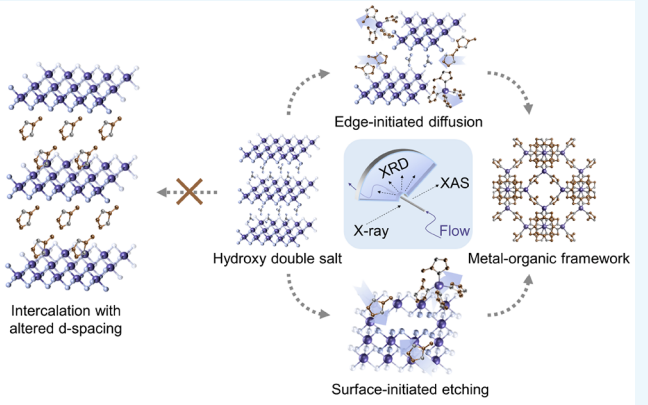

KEYWORDS: *hydroxy double salts, metal–organic frameworks, in-situ characterization, X-ray diffraction, X-ray absorption spectroscopy*

INTRODUCTION

Rapid room-temperature synthesis of metal–organic frameworks (MOFs) has been highly desired for industrial implementation of MOFs and MOF-functionalized composites.[1,2] Using hydroxy double salts (HDSs) as precursors for MOF synthesis possesses advantages including facile processing at room temperature and high space–time yield.[3] Additionally, the HDS-based method has been demonstrated on various substrates and enabled fast fabrication of functional MOF structures such as hierarchical pores MOFs,[4] MOF-coated fibers,[5] and MOF membranes.[6] However, the detailed reaction mechanism and kinetics involved in the conversion from HDS to MOF is still not fully understood, mainly due to the difficulty in obtaining direct evidence in this fast heterogeneous process. Accordingly, new HDS-based synthesis routes developed in recent years are limited. In-depth study of the transformation mechanism is therefore key to promoting further advances in new fabrication methods for MOF materials.

Up to now, several research works have investigated the dynamic process involved in the HDS-based synthesis. Zhao et al.[3,7] pioneered the study of HKUST-1 formation from (Zn,Cu) HDS using in-situ time-resolved attenuated total reflectance Fourier transform infrared (ATR-FTIR) spectroscopy. This technique excels in real-time monitoring of bond formation and anion exchange. However, ATR-FTIR falls short in probing the dynamic changes in crystal structures, leaving key kinetic information during the nucleation and growth periods unexplored. Chen et al.[8] found an intercalation state in ex-situ X-ray diffraction (XRD) patterns during the conversion from (Zn,Co) HDS to mixed-metal zeolitic imidazolate

Received: October 29, 2023
Revised: December 21, 2023
Accepted: January 28, 2024
Published: February 5, 2024

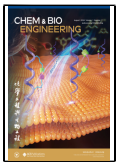

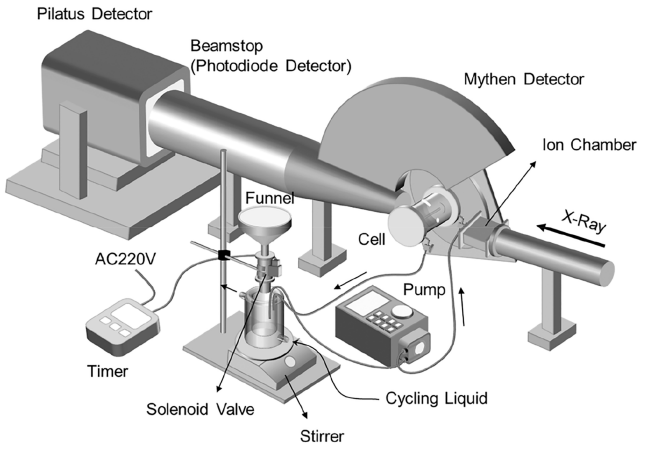

Figure 1. Schematic of the custom-built flow system for in-situ synchrotron measurements.

frameworks-7 (mmZIF-7) and thus proposed a two-step mechanism involving the intercalated intermediate. Sun et al.[9] also used ex-situ XRD to study the transformation from (Co,Co) HDS to ZIF-67. Their work revealed that the (Co,Co) HDS enabled faster nucleation than the alternatives like (Co,Al) layered double hydroxide (LDH) and $Co(OH)_2$. Nevertheless, the ex-situ approaches present limitations. Data from quenched materials may suffer from potential deviations, as there is no foolproof way to instantly halt the reaction during quenching. Residual reactants may lead to irrelevant products in the collected samples, complicating the validation of intermediate states during synthesis. These limitations underscore the urgent need for developing in-situ characterization techniques to reliably capture the dynamic conversion from HDS to MOF.

Previously, several in-situ measurements have been employed to investigate MOF synthesis, including energy-dispersive[10,11] and angle-dispersive[12,13] XRD, small-angle X-ray scattering,[14] static light scattering,[15] X-ray absorption spectroscopy (XAS),[16,17] liquid cell transmission electron microscopy,[18] atomic force microscopy,[19] quartz crystal microbalances,[20] surface plasmon resonance,[21] and magic-angle spinning nuclear magnetic resonance.[22] Most of these studies have primarily focused on solvothermal and layer-by-layer synthesis which only involved homogenous reagent solutions. On the contrary, the HDS-based synthesis starts with a heterogeneous mixture, thereby adding complexity to the design of our in-situ apparatus. The rapid conversion rate also necessitates avoiding the pre-mixing between the HDS and the ligand before data collection, in order to capture the early stage of the synthesis. Furthermore, synchronized data acquisition has emerged for obtaining consistent and corroborative evidence.[23] While the previous works carried out combined SAXS/WAXS to investigate the changes in size, shape and crystallinity during MOF formation,[15,17,24−26] simultaneous X-ray diffraction and absorption measurements are still yet to explore for unveiling the mechanisms for MOF synthesis.

Here, we reported for the first time the combination of in-situ synchrotron XRD and XAS techniques to monitor the changes in structures and coordination environment during the dynamic transformation from HDS to MOF. We chose the conversion from (Zn,Co) HDS to mmZIF-8 as our model system to investigate. In a typical process, (Zn,Co) HDS well

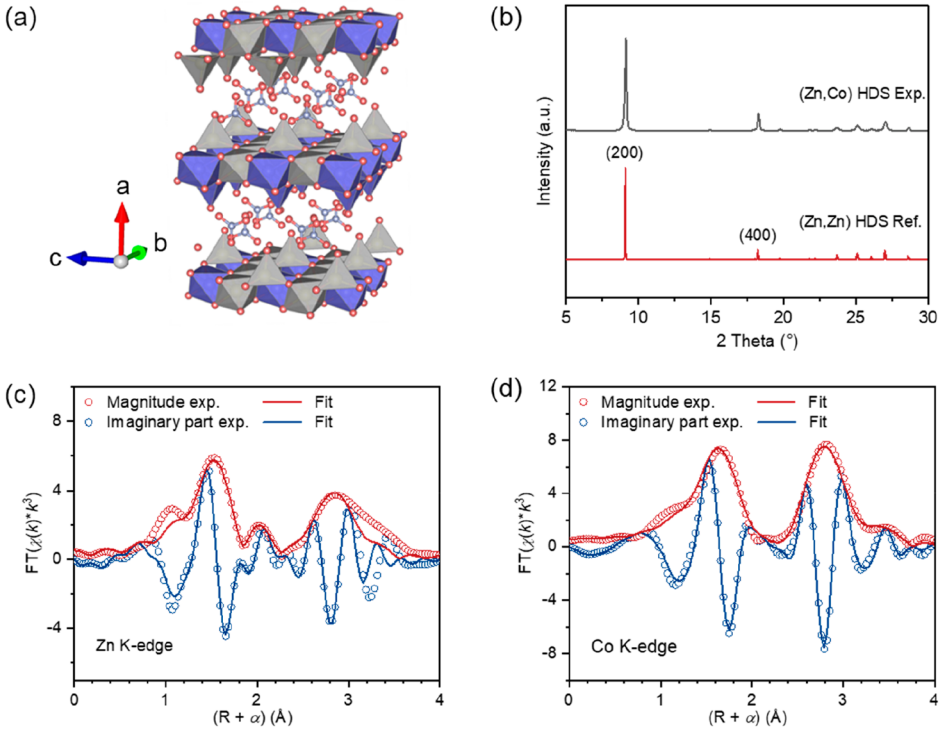

Figure 2. (a) Schematic of the layered structure of (Zn,Co) HDS. Color code: gray, Zn polyhedron; purple, Co polyhedron; silver, N atom; red, O atom. (b) XRD patterns of the obtained (Zn,Co) HDS and the reported (Zn,Zn) HDS.[29] (c) Zn K-edge EXAFS (points) and the curve fit (line) for (Zn,Co) HDS shown in R-space (FT magnitude and imaginary component). (d) Co K-edge EXAFS (points) and the curve fit (line) for (Zn,Co) HDS shown in R-space (FT magnitude and imaginary component). The data in (c) and (d) are k^3-weighted and not phase-corrected.

https://doi.org/10.1021/cbe.3c00078
Chem Bio Eng. 2024, 1, 606−614

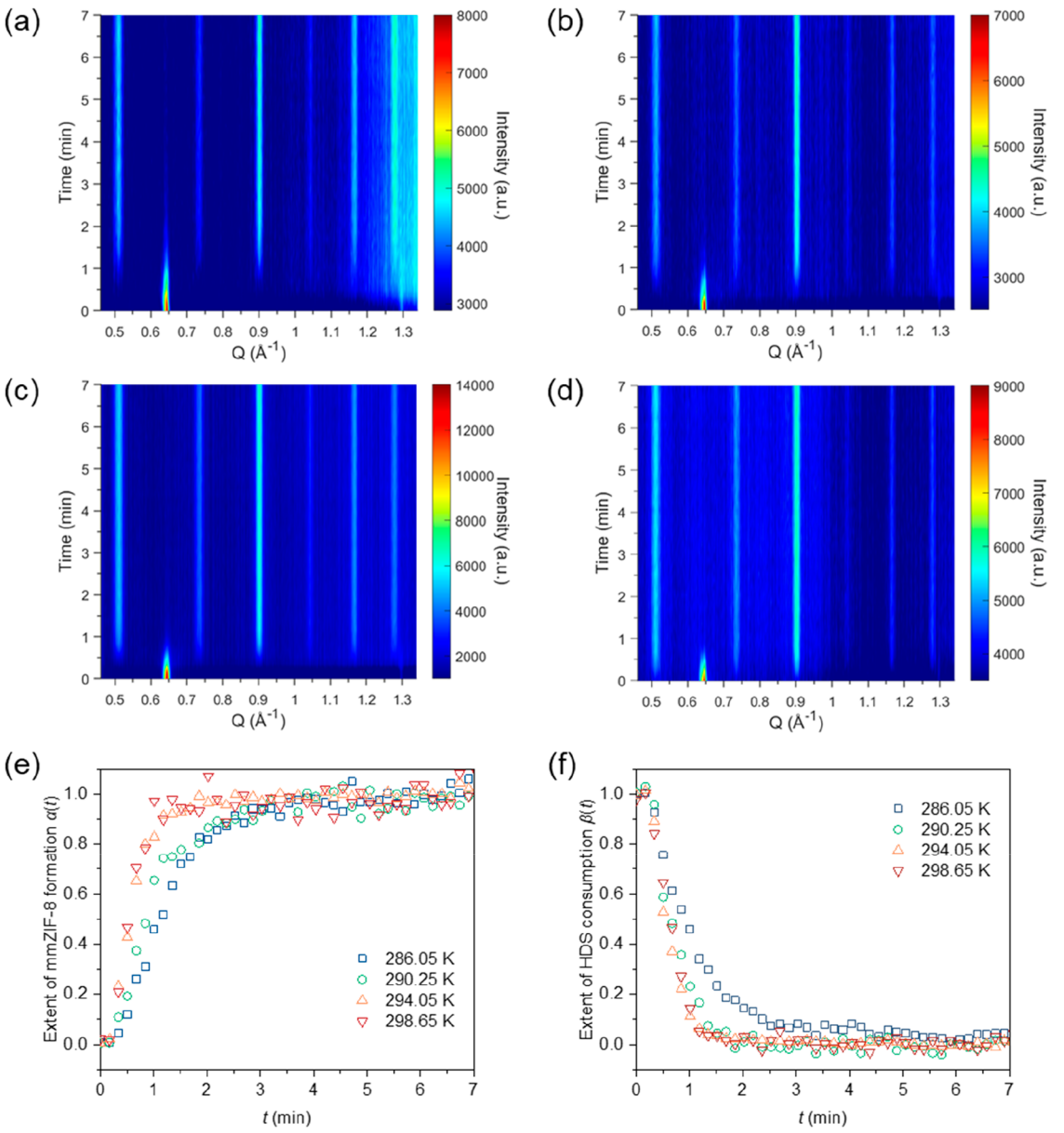

Figure 3. In-situ synchrotron XRD patterns for the conversion from (Zn,Co) HDS to mmZIF-8 measured at (a) 286.05 K, (b) 290.25 K, (c) 294.05 K, and (d) 298.65 K. (e,f) Reaction extent represented by normalized integrated peak area for (e) the mmZIF-8 (211) peak and (f) the (Zn,Co) HDS (200) peak.

dispersed in a mixed solvent of deionized water and ethanol reacted immediately upon mixing with the ethanolic solution of 2-methylimidazole (2-mIm) and rapidly converted to mmZIF-8 within minutes at room temperature. Carefully considering the challenges posed by this rapid heterogeneous system, we developed a custom-built flow system with a capillary cell (Figure 1). The small inner diameter of the capillary tube (1 mm) ensured sufficient XAS signal.[27] The external circulation system, positioned off the beam path, provides freedom of reactor customization to accommodate complicated synthesis processes. Specifically, such design allows us to add a magnetic stirrer and a timer-gated funnel to the temperature-controlled jacketed beaker. The timer-controlled solenoid valve was devised to automatically initiate the quick addition of the ligand solution from the funnel to the beaker with dispersed HDS, triggering the synthesis immediately without unnecessary pre-mixing. Taking advantage of this apparatus, we investigated the HDS-based synthesis for mmZIF-8 at different temperatures and performed kinetic analysis for the nucleation and growth periods. In addition, we studied the changes in local coordination environment and morphology and further proposed two possible pathways for the conversion from HDS to MOF.

RESULTS AND DISCUSSION

Structure Characterization of the HDS Precursor. We first characterized the structure of the (Zn,Co) HDS precursor prepared for MOF conversion using XRD and XAS measurements. The (Zn,Co) HDS was synthesized by hydrolyzing ZnO in an aqueous solution of $Co(NO_3)_2$.[28] The XRD pattern of our (Zn,Co) HDS (Figure 2b) is similar to the reported pattern for (Zn, Zn) HDS,[29] confirming the layered structure.

https://doi.org/10.1021/cbe.3c00078
Chem Bio Eng. 2024, 1, 606−614

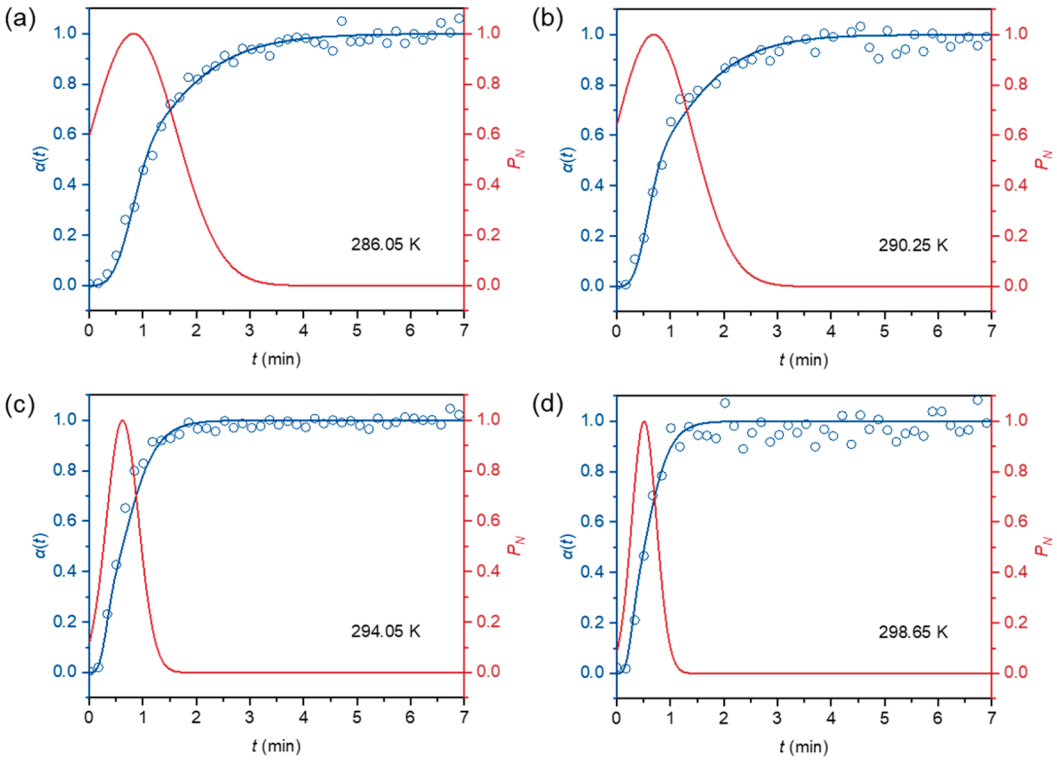

Figure 4. Fitting of the mmZIF-8 formation curve (blue circles) to the Gualtieri model (blue curve) and the resulting probability for nucleation P_N (red curve) at (a) 286.05 K, (b) 290.25 K, (c) 294.05 K, and (d) 298.65 K.

Table 1. Kinetic Parameters Obtained by Fitting mmZIF-8 Formation Curves via the Gualtieri Model

Temp (K)	a	b	k_N (min^{-1})	k_G (min^{-1})
286.05	0.83 ± 0.17	0.81 ± 0.12	1.21 ± 0.25	1.22 ± 0.11
290.25	0.69 ± 0.14	0.73 ± 0.05	1.45 ± 0.29	1.67 ± 0.10
294.05	0.62 ± 0.02	0.30 ± 0.07	1.61 ± 0.06	3.23 ± 0.37
298.65	0.51 ± 0.03	0.23 ± 0.03	1.95 ± 0.11	3.67 ± 0.14

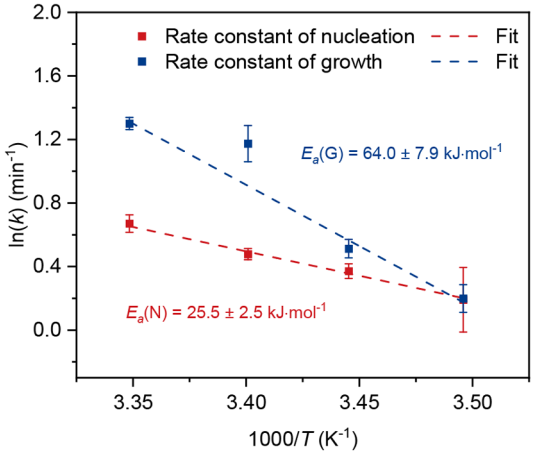

Figure 5. Arrhenius plot for the temperature-dependent rate constants of nucleation and growth obtained from the Gualtieri model.

Specifically, the peak at $2\theta = 9.12°$ corresponds to (200) planes with a d-spacing of 9.68 Å, which agrees with the literature.[28] Previously, the structures of HDSs were mainly deduced by the stoichiometric ratios and the XRD patterns.[28−32] Here, we identified the mixed coordination environment for Zn and Co in the cationic layers of (Zn,Co) HDS by fitting the extended X-ray absorption fine structure (EXAFS) data. Notably, the Zn^{2+} in the obtained HDS possesses about 68% tetrahedral coordination states and 32% octahedral coordination states. In contrast, the Co^{2+} in the (Zn,Co) HDS possesses approximately 35% tetrahedrons and 65% octahedrons, respectively. Our results reveal that cobalt doping modulates the coordination environment for Zn, which is not easily detectable by stoichiometric analysis.

Time-Resolved XRD for the Dynamic Conversion. In order to investigate the dynamic process to convert (Zn,Co) HDS to mmZIF-8 in solution, we developed a custom-built flow system for combined in-situ synchrotron XRD and XAS measurements. Figure 3a−d depict the time-resolved XRD data obtained at 286.05, 290.25, 294.05, and 298.65 K, respectively. In Figure 3a−d, the (200) peaks at $q = 0.64$ Å^{-1} associated with the HDS precursor exhibit high signal-to-noise ratio, sufficient for obtaining quality in-situ data. The rapid decrease of intensity for the HDS (200) peak within the first 2 min suggests the quick consumption of the (Zn,Co) HDS. Concurrently, the peaks at $q = 0.51$ Å^{-1} and $q = 0.90$ Å^{-1} evolved with increased intensity as the reaction progressed. The two peaks are related with the (210) and (211) planes of mmZIF-8. Energy dispersive X-ray (EDX) mapping images (Figure S3) show a uniform distribution of Zn and Co in the resulting mmZIF-8. Inductively coupled plasma-optical emission spectroscopy (ICP-OES) also reveals that the Zn:Co ratio in our mmZIF-8 (1.8:1) agrees well with the (Zn,Co) HDS precursor (Table S7), suggesting a stoichiometric transformation.[8] Previously, the expansion of the interlayer spacing has been commonly found in the HDSs intercalated by various organic linkers[33,34] and observed in the

https://doi.org/10.1021/cbe.3c00078
Chem Bio Eng. 2024, 1, 606−614

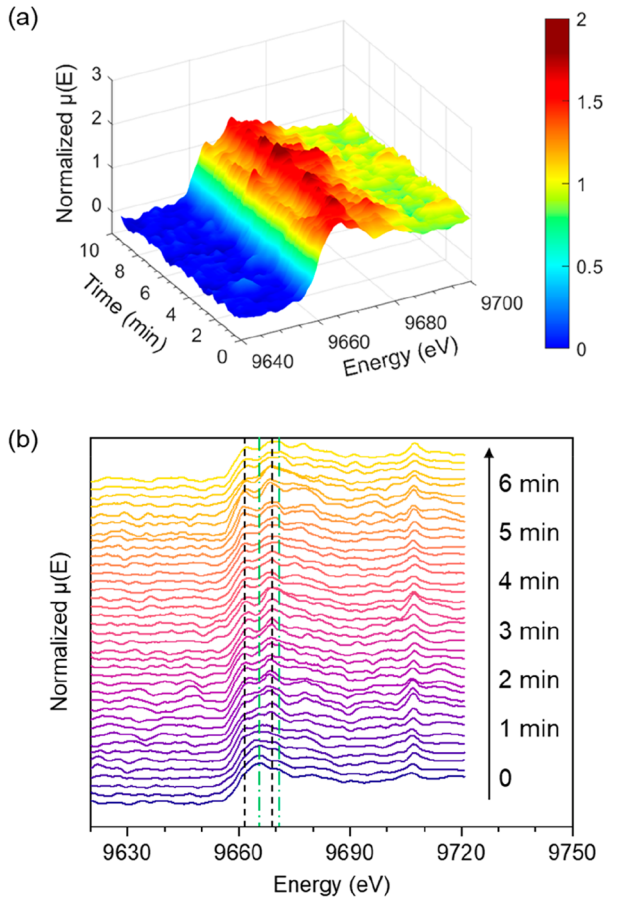

Figure 6. (a) Normalized in-situ Zn K-edge XANES spectra of the conversion from (Zn,Co) HDS to mmZIF-8 at 288.85 K. (b) Processed in-situ Zn K-edge XANES spectra of the conversion from (Zn,Co) HDS to mmZIF-8 at 288.85 K. The green dot-dash lines refer to the mixed octahedral and tetrahedral coordination in (Zn,Co) HDS. The black dash lines refer to the tetrahedral coordination in mmZIF-8.

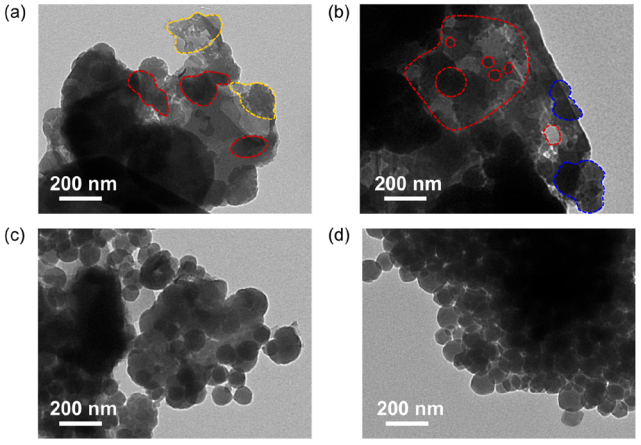

Figure 7. TEM images of the solids collected after the HDS was exposed to the ligand solution for (a) 30 s (agglomerates and fragments highlighted in red and yellow dashed circles, respectively), (b) 1 min (mmZIF-8 particles along the HDS edges highlighted in blue dashed circles; mmZIF-8 structures on the surface of the HDS sheets as well as the pit and hole structures highlighted in red dashed circles.), (c) 3 min, and (d) 5 min at 298.65 K.

collected solid species by ex-situ XRD measurements.[8] In contrast, no change in *d*-spacing was found in our work, indicating negligible intercalation by 2-mIm linkers prior to the conversion of the HDS to mmZIF-8. This finding further suggests a possible diffusion-controlled process, where the reaction rate to form mmZIF-8 was substantially faster than the diffusion rate of 2-mIm linkers into the interlayer spaces of the (Zn,Co) HDS.

We further performed quantitative analysis to study the reaction kinetics. Here, we define t as the reaction time (in units of min), the extent of mmZIF-8 formation, $\alpha(t)$, as the integrated peak area $I_{ZIF}(t)$ normalized by the maximum integrated peak area $I_{max,ZIF}$ for the mmZIF-8 (211) peak (eq 1), and the extent of HDS consumption, $\beta(t)$, as the integrated peak area $I_{HDS}(t)$ normalized by the maximum integrated peak area $I_{max,HDS}$ for the HDS (200) peak, respectively (eq 2).

$$\alpha(t) = \frac{I_{ZIF}(t)}{I_{max,ZIF}} \tag{1}$$

$$\beta(t) = \frac{I_{HDS}(t)}{I_{max,HDS}} \tag{2}$$

Figure 3 panels e and f show that $\alpha(t)$ increases rapidly in the first few minutes before reaching a plateau at all the four temperatures while $\beta(t)$ decreases simultaneously until the HDS is fully converted during the synthesis. Notably, the extent of reaction reached 95% in just ca. 3 min, even at temperatures as low as 286.05 K. Compared to conventional solvothermal synthesis[35] which takes hours to days, this HDS-based synthesis exhibits advantages in rapid conversion and low synthesis temperatures.

Kinetic Modeling. To further explore the kinetic information of the reaction, mathematical models were employed to analyze the nucleation and growth behaviors. Previously, several models have been proposed by Avrami and Erofeev,[36−38] Sharp and Hancock,[39] and Gualtieri[40] for describing crystallization processes. Here, the Gualtieri model (eq 3) was chosen because of its capability to describe heterogeneous reactions and decouple the nucleation and growth processes.[40] Analyses carried out using other models were also given in the Supporting Information (Figures S7−S10, Tables S1 and S2) for comparison.

$$\alpha(t) = \frac{1}{1 + e^{-(t-a)/b}}[1 - e^{-(k_G \cdot t)^n}] \tag{3}$$

$$P_N = \frac{dN}{dt} = e^{-(t-a)^2/2b^2} \tag{4}$$

$$k_N = \frac{1}{a} \tag{5}$$

In the Gualtieri equation, $\alpha(t)$ depends on the rate constant of growth (k_G, in units of min^{-1}), the fitting parameter a and b, along with the dimensionality of crystal growth (n), which is set to 3 in most cases of MOF crystallization.[10,11,35,41] The probability of nucleation (P_N) is defined as the amount of nuclei (N) found at time t and is given as a function of the parameter a and b (eq 4). Furthermore, the rate constant of nucleation (k_N, in units of min^{-1}) is given as the reciprocal of the parameter a (eq 5).

Figure 4 panels a−d show the fitting plots of $\alpha(t)$ and P_N versus time t at four different temperatures. The corresponding

https://doi.org/10.1021/cbe.3c00078
Chem Bio Eng. 2024, 1, 606−614

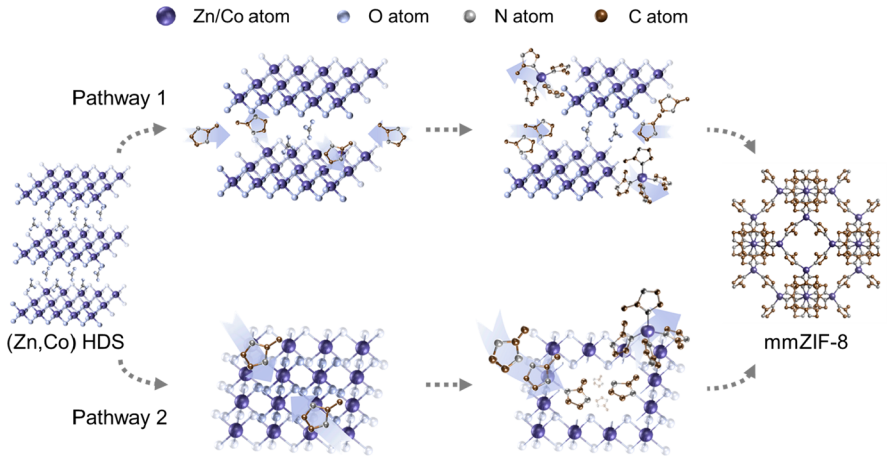

Figure 8. Schematic of two proposed reaction pathways. The layered structures of the HDS are simplified as planar sheets consisting of octahedral coordination nodes only. H atoms are omitted for clarity.

kinetic parameters in these cases are summarized in Table 1. We found that the rate constants for nucleation and growth both increase with the rise of temperature. The narrower peak widths in these $P_N - t$ profiles, along with earlier P_N maximums, also indicate the temperature dependence of the nucleation rates.[35]

We obtained the activation energy E_a of nucleation and growth by applying a linear fitting to the Arrhenius equation (eq 6), and found E_a(N) and E_a(G) during the HDS-based synthesis to be 25.5 ± 2.5 and 64.0 ± 7.9 kJ·mol^{-1}, respectively (Figure 5). The activation energy of nucleation obtained here is lower than common synthesis reactions to prepare MOFs in literature,[10,35,41−44] suggesting a reduced energy barrier for MOF formation by our method.

$$k = Ae^{-E_a/RT} \tag{6}$$

Local Structure Evolution During the HDS Conversion. Furthermore, in-situ X-ray absorption spectroscopy reveals the changes in the local coordination environment for the metal nodes during the transformation from (Zn,Co) HDS to mmZIF-8. Since the raw data exhibit low signal-to-noise ratio with a temporal resolution of 9.5 s, we superposed every three neighboring spectra to enhance the signal quality (Figure 6a, details provided in the Supporting Information). Figure 6b shows the processed X-ray absorption near edge structures (XANES) data collected at Zn K-edge in the first 6.5 min of reaction. The energy position of the rising edge, associated with the 1s to 4p electron transition, is closely related to the valence state of the corresponding metal in the material.[45,46] We found that the edge positions remained unchanged during the entire HDS conversion, indicating no redox to the zinc ions. The first spectrum in the series of processed in-situ spectra (Figure 6b) shows a major peak at 9665.2 eV, followed by a minor peak at 9670.2 eV. These peaks represent the mixed octahedral and tetrahedral coordination for Zn^{2+} in (Zn,Co) HDS, which also agree well with the XANES spectrum collected ex situ (Figure S13a). Notably, these peaks significantly diminished after ca. 1 min of reaction, which indicates the fast consumption of the sheet structure in HDS. Simultaneously, the evolution of new peaks at 9662.2 and 9668.7 eV was observed, confirming the formation of tetrahedrally coordinated species identical to the secondary building units (SBUs) in ZIF-8.[47,48] Previously, in homogeneous solutions for solvothermal synthesis, the formation of ZIF-8 has been generally considered to involve assembly of linkers and free Zn aqua ions that possess octahedral coordination identified with a single peak at 9667 eV.[18,49] However, our results suggest that tetrahedral-coordinated SBUs are more likely generated via direct conversion from the HDS cationic hydroxide sheets rather than free aqua ions.

Morphological Changes and Proposed Mechanism. The transmission electron microscopy (TEM) images in Figure 7 reveal the morphological changes during the conversion from HDS to ZIF at 298.65 K. We isolated these solids by quenching the reaction after predetermined time intervals. The sheet-like morphology of pristine HDS is shown in Figure S3a. We observed agglomerates of irregular shapes formed around the HDS in the solids collected after 30 s of reaction (Figure 7a), which possibly correspond to nascent mmZIF-8 based on the above-mentioned in-situ XRD results. Additionally, fragments with size of ca. 20 nm were found in Figure 7a. Due to the TEM contrast similar to the HDS, we infer that these fragments were generated from the scissoring of HDS sheets by 2-mIm ligands. Such a process may accelerate the transformation into mmZIF-8. In Figure 7b, we found continuously grown mmZIF-8 particles along the HDS edges. Such growth behavior provides further evidence of a diffusion-controlled process as proposed in the in-situ XRD analysis. Moreover, we identified pit and hole structures on the surface of the HDS, accompanied by small mmZIF-8 nuclei (Figure 7b). These features suggest a surface-initiated etch process, likely to expose more reactive sites in the HDS sheets to the ligands and contribute to the formation of numerous SBUs. Figure 7 panels c and d show a substantially decreased fraction of HDS in the collected solids as the reaction progressed. Concurrently, the formed mmZIF-8 particles evolved into well-faceted rhombic dodecahedral shapes, resembling the morphology of monometallic ZIF-8.[44] Based on the TEM observation and the above-mentioned in-situ synchrotron characterization results, we have proposed two possible reaction pathways as shown in Figure 8, which both contribute to the fast conversion rate: (1) In Pathway 1, linkers diffusing into the interlayer spacing react with the cationic hydroxy sheets to form MOF SBUs. (2) In Pathway 2, surface-initiated etching induces the fragmentation of HDS sheets and exposes more sites for SBU formation and MOF nucleation. The general transformation of (Zn, Co) HDS to mixed-metal ZIFs has been reported,[8] and was further substantiated by a

https://doi.org/10.1021/cbe.3c00078
Chem Bio Eng. 2024, 1, 606−614

new synthesis route to form mixed-metal ZIF-65 (Figure S15) developed in this work.

CONCLUSION

In summary, we have reported for the first time the use of combined synchrotron XRD and XAS techniques for in-situ monitoring a MOF synthesis. A custom-built flow system has been designed and installed on the beamline for investigating a model reaction to convert (Zn,Co) HDS to mmZIF-8. Time-resolved diffraction patterns show that, even at temperatures as low as 286.05 K, over 95% conversion was achieved in 3 min. In contrast to the findings obtained by past ex-situ measurements, our in-situ XRD results exclude the presence of intercalated HDS structure as an intermediate state during the synthesis. Kinetic analysis using the Gualtieri model reveals that the activation energies of nucleation and growth are 25.5 ± 2.5 and 64.0 ± 7.9 kJ·mol^{-1}, respectively. In addition, we found a transformation of local structure from mixed coordination state in the HDS to tetrahedral coordination in the mmZIF-8 via in-situ XANES. Based on the structural and morphological changes, we proposed two possible reaction pathways facilitating the formation of mmZIF-8. Our results provide important insights into the HDS-based synthesis and are expected to promote further advances of new fabrication routes for MOF materials.

ASSOCIATED CONTENT

Supporting Information

The Supporting Information is available free of charge at https://pubs.acs.org/doi/10.1021/cbe.3c00078.

Experimental details, materials characterization, and kinetic modeling results, figures showing photos of the equipment, mixed coordination environment, TEM and EDX mapping images, XRD patterns, FTIR spectra, photos and SEM images of the solids collected, fitting of the mmZIF-8 formation curve to the Avrami−Erofeev model and to the Sharp−Hancock equation, Arrhenius plots for the temperature-dependent rate constants, in-situ synchrotron XRD spectra, formation and consumption curves, normalized ex-situ XANES spectra, N_2 adsorption isotherms and pore size distributions, and tables of kinetic parameters, curve fit parameters, ratios of different geometries, and Zn:Co ratios (PDF)

AUTHOR INFORMATION

Corresponding Author

Junjie Zhao − *State Key Laboratory of Chemical Engineering, College of Chemical and Biological Engineering, Zhejiang University, Hangzhou, Zhejiang 310058, P. R. China; Institute of Zhejiang University - Quzhou, Quzhou, Zhejiang 324000, P. R. China;* orcid.org/0000-0001-6205-9671; Email: junjiezhao@zju.edu.cn

Authors

Ming Zhang − *State Key Laboratory of Chemical Engineering, College of Chemical and Biological Engineering, Zhejiang University, Hangzhou, Zhejiang 310058, P. R. China; Institute of Zhejiang University - Quzhou, Quzhou, Zhejiang 324000, P. R. China*

Xinyu Luo − *State Key Laboratory of Chemical Engineering, College of Chemical and Biological Engineering, Zhejiang University, Hangzhou, Zhejiang 310058, P. R. China; Institute of Zhejiang University - Quzhou, Quzhou, Zhejiang 324000, P. R. China*

Yubin Hu − *State Key Laboratory of Chemical Engineering, College of Chemical and Biological Engineering, Zhejiang University, Hangzhou, Zhejiang 310058, P. R. China; Institute of Zhejiang University - Quzhou, Quzhou, Zhejiang 324000, P. R. China*

Yuanhao Shen − *State Key Laboratory of Chemical Engineering, College of Chemical and Biological Engineering, Zhejiang University, Hangzhou, Zhejiang 310058, P. R. China; Institute of Zhejiang University - Quzhou, Quzhou, Zhejiang 324000, P. R. China*

Yixin Chen − *State Key Laboratory of Chemical Engineering, College of Chemical and Biological Engineering, Zhejiang University, Hangzhou, Zhejiang 310058, P. R. China; Institute of Zhejiang University - Quzhou, Quzhou, Zhejiang 324000, P. R. China*

Shuchang Yuan − *State Key Laboratory of Chemical Engineering, College of Chemical and Biological Engineering, Zhejiang University, Hangzhou, Zhejiang 310058, P. R. China; Institute of Zhejiang University - Quzhou, Quzhou, Zhejiang 324000, P. R. China*

Hao Wang − *Beijing Synchrotron Radiation Facility, Institute of High Energy Physics, Chinese Academy of Sciences, Beijing 100049, P. R. China*

Xueqing Xing − *Beijing Synchrotron Radiation Facility, Institute of High Energy Physics, Chinese Academy of Sciences, Beijing 100049, P. R. China;* orcid.org/0000-0002-1052-6319

Complete contact information is available at: https://pubs.acs.org/10.1021/cbe.3c00078

Notes

The authors declare no competing financial interest.

ACKNOWLEDGMENTS

All authors acknowledge the funding from the National Natural Science Foundation of China (21908194, 21938011 and 22178301) and the funding from the Natural Science Foundation of Zhejiang Province (LR21B060003). J.Z. is also grateful for the grant from the Science & Technology Department of Zhejiang Province (2023C01182). This work is also supported by the Shanxi Institute of Zhejiang University for New Materials and Chemical Industry (2022SZ-TD005) and the Quzhou Science and Technology Program (2021NC02). The XRD/XAS beam time was granted by beamline 1W2B and 4B9A of Beijing Synchrotron Radiation Facility, Institute of High Energy Physics, Chinese Academy of Sciences. The staff members of 1W2B and 4B9A are acknowledged for their support in measurements.

REFERENCES

(1) Stock, N.; Biswas, S. Synthesis of Metal-Organic Frameworks (MOFs): Routes to Various MOF Topologies, Morphologies, and Composites. *Chem. Rev.* **2012**, *112* (2), 933−969.

(2) Ren, J.; Dyosiba, X.; Musyoka, N. M.; Langmi, H. W.; Mathe, M.; Liao, S. Review on the Current Practices and Efforts towards Pilot-Scale Production of Metal-Organic Frameworks (MOFs). *Coord. Chem. Rev.* **2017**, *352*, 187−219.

(3) Zhao, J.; Nunn, W. T.; Lemaire, P. C.; Lin, Y.; Dickey, M. D.; Oldham, C. J.; Walls, H. J.; Peterson, G. W.; Losego, M. D.; Parsons, G. N. Facile Conversion of Hydroxy Double Salts to Metal-Organic Frameworks Using Metal Oxide Particles and Atomic Layer

Deposition Thin-Film Templates. *J. Am. Chem. Soc.* **2015**, *137* (43), 13756−13759.
(4) Duan, C.; Li, F.; Li, L.; Zhang, H.; Wang, X.; Xiao, J.; Xi, H. Hierarchically Structured Metal-Organic Frameworks Assembled by Hydroxy Double Salt-Template Synergy with High Space-Time Yields. *CrystEngComm* **2018**, *20* (8), 1057−1064.
(5) Lee, D. T.; Jamir, J. D.; Peterson, G. W.; Parsons, G. N. Water-Stable Chemical-Protective Textiles via Euhedral Surface-Oriented 2D Cu-TCPP Metal-Organic Frameworks. *Small* **2019**, *15* (10), 1805133.
(6) Ma, C.; Gao, G.; Liu, H.; Liu, Y.; Zhang, X. Fabrication of 2D Bimetallic Metal-Organic Framework Ultrathin Membranes by Vapor Phase Transformation of Hydroxy Double Salts. *J. Membr. Sci.* **2022**, *644*, 120167.
(7) Zhao, J.; Kalanyan, B.; Barton, H. F.; Sperling, B. A.; Parsons, G. N. In Situ Time-Resolved Attenuated Total Reflectance Infrared Spectroscopy for Probing Metal-Organic Framework Thin Film Growth. *Chem. Mater.* **2017**, *29* (20), 8804−8810.
(8) Chen, Y.; Yuan, S.; Li, Y.; Ma, Y.; Zhang, C.; Zhang, M.; Mao, Q.; Luo, Y.; Zhao, J. Pre-Programed Hydroxy Double Salt Templates for Room-Temperature Controlled Synthesis of Mixed-Metal Zeolitic Imidazolate Frameworks. *J. Mater. Chem. A* **2021**, *9* (34), 18557−18563.
(9) Sun, H.; Wang, F.; Li, X.; Caro, J.; Meng, H.; Wang, N.; An, Q. Facile Fabrication of a Continuous ZIF-67 Membrane for Efficient Azeotropic Organic Solvent Mixture Separation. *Angew. Chem. Int. Ed.* **2023**, *62* (15), No. e202300262.
(10) Zahn, G.; Zerner, P.; Lippke, J.; Kempf, F. L.; Lilienthal, S.; Schröder, C. A.; Schneider, A. M.; Behrens, P. Insight into the Mechanism of Modulated Syntheses: In Situ Synchrotron Diffraction Studies on the Formation of Zr-Fumarate MOF. *CrystEngComm* **2014**, *16* (39), 9198−9207.
(11) Ragon, F.; Horcajada, P.; Chevreau, H.; Hwang, Y. K.; Lee, U.-H.; Miller, S. R.; Devic, T.; Chang, J.-S.; Serre, C. In Situ Energy-Dispersive X-Ray Diffraction for the Synthesis Optimization and Scale-up of the Porous Zirconium Terephthalate UiO-66. *Inorg. Chem.* **2014**, *53* (5), 2491−2500.
(12) Wu, Y.; Henke, S.; Kieslich, G.; Schwedler, I.; Yang, M.; Fraser, D. A. X.; O'Hare, D. Time-Resolved In Situ X-Ray Diffraction Reveals Metal-Dependent Metal-Organic Framework Formation. *Angew. Chem. Int. Ed.* **2016**, *55* (45), 14081−14084.
(13) Wu, Y.; Moorhouse, S. J.; O'Hare, D. Time-Resolved *in Situ* Diffraction Reveals a Solid-State Rearrangement During Solvothermal MOF Synthesis. *Chem. Mater.* **2015**, *27* (21), 7236−7239.
(14) Sang, X.; Zhang, J.; Xiang, J.; Cui, J.; Zheng, L.; Zhang, J.; Wu, Z.; Li, Z.; Mo, G.; Xu, Y.; Song, J.; Liu, C.; Tan, X.; Luo, T.; Zhang, B.; Han, B. Ionic Liquid Accelerates the Crystallization of Zr-Based Metal-Organic Frameworks. *Nat. Commun.* **2017**, *8* (1), 175.
(15) Saha, S.; Springer, S.; Schweinefuß, M. E.; Pontoni, D.; Wiebcke, M.; Huber, K. Insight into Fast Nucleation and Growth of Zeolitic Imidazolate Framework-71 by In Situ Time-Resolved Light and X-Ray Scattering Experiments. *Cryst. Growth Des.* **2016**, *16* (4), 2002−2010.
(16) Semivrazhskaya, O. O.; Salionov, D.; Clark, A. H.; Casati, N. P. M.; Nachtegaal, M.; Ranocchiari, M.; Bjelić, S.; Verel, R.; van Bokhoven, J. A.; Sushkevich, V. L. Deciphering the Mechanism of Crystallization of UiO-66 Metal-Organic Framework. *Small* **2023**, *19* (52), 2305771.
(17) Goesten, M.; Stavitski, E.; Pidko, E. A.; Gücüyener, C.; Boshuizen, B.; Ehrlich, S. N.; Hensen, E. J. M.; Kapteijn, F.; Gascon, J. The Molecular Pathway to ZIF-7 Microrods Revealed by In Situ Time-Resolved Small- and Wide-Angle X-Ray Scattering, Quick-Scanning Extended X-Ray Absorption Spectroscopy, and DFT Calculations. *Chem.—Eur. J.* **2013**, *19* (24), 7809−7816.
(18) Patterson, J. P.; Abellan, P.; Denny, M. S.; Park, C.; Browning, N. D.; Cohen, S. M.; Evans, J. E.; Gianneschi, N. C. Observing the Growth of Metal-Organic Frameworks by *in Situ* Liquid Cell Transmission Electron Microscopy. *J. Am. Chem. Soc.* **2015**, *137* (23), 7322−7328.
(19) Shoaee, M.; Anderson, M. W.; Attfield, M. P. Crystal Growth of the Nanoporous Metal-Organic Framework HKUST-1 Revealed by In Situ Atomic Force Microscopy. *Angew. Chem. Int. Ed.* **2008**, *47* (44), 8525−8528.
(20) Stavila, V.; Volponi, J.; Katzenmeyer, A. M.; Dixon, M. C.; Allendorf, M. D. Kinetics and Mechanism of Metal-Organic Framework Thin Film Growth: Systematic Investigation of HKUST-1 Deposition on QCM Electrodes. *Chem. Sci.* **2012**, *3* (5), 1531−1540.
(21) Shekhah, O.; Wang, H.; Zacher, D.; Fischer, R. A.; Wöll, C. Growth Mechanism of Metal-Organic Frameworks: Insights into the Nucleation by Employing a Step-by-Step Route. *Angew. Chem. Int. Ed.* **2009**, *48* (27), 5038−5041.
(22) Salionov, D.; Semivrazhskaya, O. O.; Casati, N. P. M.; Ranocchiari, M.; Bjelić, S.; Verel, R.; Van Bokhoven, J. A.; Sushkevich, V. L. Unraveling the Molecular Mechanism of MIL-53(Al) Crystallization. *Nat. Commun.* **2022**, *13* (1), 3762.
(23) Wu, Z.; Liu, Y.; Xing, X.; Yao, L.; Chen, Z.; Mo, G.; Zheng, L.; Cai, Q.; Wang, H.; Zhong, J.; Lai, Y.; Qian, L. A Novel SAXS/XRD/XAFS Combined Technique for in-Situ Time-Resolved Simultaneous Measurements. *Nano Res.* **2023**, *16* (1), 1123−1131.
(24) Stavitski, E.; Goesten, M.; Juan-Alcañiz, J.; Martinez-Joaristi, A.; Serra-Crespo, P.; Petukhov, A. V.; Gascon, J.; Kapteijn, F. Kinetic Control of Metal-Organic Framework Crystallization Investigated by Time-Resolved In Situ X-Ray Scattering. *Angew. Chem. Int. Ed.* **2011**, *50* (41), 9624−9628.
(25) Zhang, P.; Kang, X.; Tao, L.; Zheng, L.; Xiang, J.; Duan, R.; Li, J.; Chen, P.; Xing, X.; Mo, G.; Wu, Z.; Han, B. A New Route for the Rapid Synthesis of Metal-Organic Frameworks at Room Temperature. *CCS Chem.* **2023**, *5* (6), 1462−1469.
(26) Cravillon, J.; Schröder, C. A.; Nayuk, R.; Gummel, J.; Huber, K.; Wiebcke, M. Fast Nucleation and Growth of ZIF-8 Nanocrystals Monitored by Time-Resolved In Situ Small-Angle and Wide-Angle X-Ray Scattering. *Angew. Chem. Int. Ed.* **2011**, *50* (35), 8067−8071.
(27) Wang, H.; Mo, G.; Zhong, J.; Liu, Y.; Qian, L.; Yao, L.; Xing, X.; Chen, Z.; Wu, Z. A Capillary Sample Cell Used for In-Situ SAXS, XRD, and XAFS Measurements during Hydrothermal Synthesis. *Nucl. Instrum. Methods Phys. Res., Sect. A* **2022**, *1031*, 166605.
(28) Meyn, M.; Beneke, K.; Lagaly, G. Anion-Exchange Reactions of Hydroxy Double Salts. *Inorg. Chem.* **1993**, *32* (7), 1209−1215.
(29) Stählin, W.; Oswald, H. R. The Crystal Structure of Zinc Hydroxide Nitrate, Zn5(OH)8(NO3)2.2H2O. *Acta Cryst. B* **1970**, *26* (6), 860−863.
(30) Allmann, R. The Crystal Structure of Pyroaurite. *Acta Cryst. B* **1968**, *24* (7), 972−977.
(31) Stählin, W.; Oswald, H. R. The Topotactic Reaction of Zinc Hydroxide Nitrate with Aqueous Metal Chloride Solutions. *J. Solid State Chem.* **1971**, *3* (2), 256−264.
(32) Morioka, H.; Tagaya, H.; Karasu, M.; Kadokawa, J.; Chiba, K. Effects of Zinc on the New Preparation Method of Hydroxy Double Salts. *Inorg. Chem.* **1999**, *38* (19), 4211−4216.
(33) Williams, G. R.; Crowder, J.; Burley, J. C.; Fogg, A. M. The Selective Intercalation of Organic Carboxylates and Sulfonates into Hydroxy Double Salts. *J. Mater. Chem.* **2012**, *22* (27), 13600.
(34) Morioka, H.; Tagaya, H.; Karasu, M.; Kadokawa, J.; Chiba, K. Preparation of Hydroxy Double Salts Exchanged by Organic Compounds. *J. Mater. Res.* **1998**, *13* (4), 848−851.
(35) Moh, P. Y.; Brenda, M.; Anderson, M. W.; Attfield, M. P. Crystallisation of Solvothermally Synthesised ZIF-8 Investigated at the Bulk, Single Crystal and Surface Level. *CrystEngComm* **2013**, *15* (45), 9672−9678.
(36) Avrami, M. Kinetics of Phase Change. I General Theory. *J. Chem. Phys.* **1939**, *7* (12), 1103−1112.
(37) Avrami, M. Kinetics of Phase Change. II Transformation-Time Relations for Random Distribution of Nuclei. *J. Chem. Phys.* **1940**, *8* (2), 212−224.
(38) Avrami, M. Granulation, Phase Change, and Microstructure Kinetics of Phase Change. III. *J. Chem. Phys.* **1941**, *9* (2), 177−184.

https://doi.org/10.1021/cbe.3c00078
Chem Bio Eng. 2024, 1, 606−614

(39) Hancock, J. D.; Sharp, J. H. Method of Comparing Solid-State Kinetic Data and Its Application to the Decomposition of Kaolinite, Brucite, and BaCO3. *J. Am. Ceram. Soc.* **1972**, *55* (2), 74−77.
(40) Gualtieri, A. F. Synthesis of Sodium Zeolites from a Natural Halloysite. *Phys. Chem. Miner.* **2001**, *28* (10), 719−728.
(41) Bagi, S. D.; Myerson, A. S.; Román-Leshkov, Y. Solvothermal Crystallization Kinetics and Control of Crystal Size Distribution of MOF-808 in a Continuous Flow Reactor. *Cryst. Growth Des.* **2021**, *21* (11), 6529−6536.
(42) Reinsch, H.; Stock, N. Formation and Characterisation of Mn-MIL-100. *CrystEngComm* **2013**, *15* (3), 544−550.
(43) Millange, F.; El Osta, R.; Medina, M. E.; Walton, R. I. A Time-Resolved Diffraction Study of a Window of Stability in the Synthesis of a Copper Carboxylate Metal-Organic Framework. *CrystEngComm* **2011**, *13* (1), 103−108.
(44) Cravillon, J.; Schröder, C. A.; Bux, H.; Rothkirch, A.; Caro, J.; Wiebcke, M. Formate Modulated Solvothermal Synthesis of ZIF-8 Investigated Using Time-Resolved in Situ X-Ray Diffraction and Scanning Electron Microscopy. *CrystEngComm* **2012**, *14* (2), 492−498.
(45) Baker, M. L.; Mara, M. W.; Yan, J. J.; Hodgson, K. O.; Hedman, B.; Solomon, E. I. K- and L-Edge X-Ray Absorption Spectroscopy (XAS) and Resonant Inelastic X-Ray Scattering (RIXS) Determination of Differential Orbital Covalency (DOC) of Transition Metal Sites. *Coord. Chem. Rev.* **2017**, *345*, 182−208.
(46) Guan, D.; Zhang, K.; Hu, Z.; Wu, X.; Chen, J.-L.; Pao, C.-W.; Guo, Y.; Zhou, W.; Shao, Z. Exceptionally Robust Face-Sharing Motifs Enable Efficient and Durable Water Oxidation. *Adv. Mater.* **2021**, *33* (41), 2103392.
(47) Hillman, F.; Zimmerman, J. M.; Paek, S.-M.; Hamid, M. R. A.; Lim, W. T.; Jeong, H.-K. Rapid Microwave-Assisted Synthesis of Hybrid Zeolitic-Imidazolate Frameworks with Mixed Metals and Mixed Linkers. *J. Mater. Chem. A* **2017**, *5* (13), 6090−6099.
(48) Butova, V. V.; Polyakov, V. A.; Budnyk, A. P.; Aboraia, A. M.; Bulanova, E. A.; Guda, A. A.; Reshetnikova, E. A.; Podkovyrina, Y. S.; Lamberti, C.; Soldatov, A. V. Zn/Co ZIF Family: MW Synthesis, Characterization and Stability upon Halogen Sorption. *Polyhedron* **2018**, *154*, 457−464.
(49) Buzanich, A. G.; Kulow, A.; Kabelitz, A.; Grunewald, C.; Seidel, R.; Chapartegui-Arias, A.; Radtke, M.; Reinholz, U.; Emmerling, F.; Beyer, S. Observation of Early ZIF-8 Crystallization Stages with X-Ray Absorption Spectroscopy. *Soft Matter* **2021**, *17* (2), 331−334.

https://doi.org/10.1021/cbe.3c00078
Chem Bio Eng. 2024, 1, 606−614